A&A 368, 52–63 (2001)
DOI: 10.1051/0004-6361:20000523

Astronomy & Astrophysics

Dynamics of embedded bars and the connection with AGN⋆

I. ISAAC/VLT stellar kinematics

E. Emsellem[1], D. Greusard[2], F. Combes[3], D. Friedli[2,6], S. Leon[4], E. Pécontal[1], and H. Wozniak[5]

[1] Centre de Recherche Astronomique de Lyon, 9 Av. Charles André, 69561 Saint-Genis Laval Cedex, France
[2] Observatoire de Genève, 1290 Sauverny, Switzerland
[3] DEMIRM, Observatoire de Paris, 61 avenue de l'Observatoire, 75014 Paris, France
[4] Institute of Astronomy and Astrophysics, Academia Sinica, PO Box 1-87, Nankang, Taipei, Taiwan, R.O.C.
[5] Observatoire de Marseille-Provence, Laboratoire d'Astrophysique de Marseille, 2 place Le Verrier, 13248 Marseille Cedex 4, France
[6] Gymnase de Nyon, 1260 Nyon, Switzerland

Received 27 October 2000 / Accepted 19 December 2000

Abstract. We present new stellar kinematical profiles of four galaxy hosts of active galactic nuclei, using the ^{12}CO bandhead around 2.3 μm with the ISAAC/VLT spectrograph. We find that the nuclear bars or discs, embedded in large-scale primary bars, have all a decoupled kinematics, in the sense that the maximum of the rotational velocity occurs in the nuclear region. In three cases (NGC 1097, NGC 1808 and NGC 5728), the velocity dispersion displays a significant drop at the nucleus, a rarely observed phenomenon. We also detect kinematical asymmetries ($m = 1$ mode) along the nuclear bar major-axis of NGC 1808 and NGC 5728, dynamical counterparts of corresponding asymmetries in the surface brightness. We have derived simple dynamical models in an attempt to fit the kinematics of each galaxy and reconstruct the full velocity field. For all four targets, the fits are good, and confirm the presence of the decoupled nuclear components. These models cannot however reproduce the observed central drop in the dispersion. We suggest that this drop is due to a transient cold nuclear disc, fuelled by gas inflow along the bar, that has recently formed new stars.

Key words. galaxies: active – galaxies: kinematics and dynamics – galaxies: nuclei – galaxies: Seyfert – galaxies: evolution – galaxies: spiral

1. Introduction

It is now widely accepted that the energy source of active galactic nuclei (AGN) originates in the accretion of material onto a central massive black hole. However, the fuelling mechanism of the central engine remains unclear. The problem is how to transfer mass from the galaxy into its very central regions (parsec scale). Several mechanisms can be invoked to induce the potential perturbation that could initiate gas inflow. Among them, $m = 2$ or $m = 1$ modes tiggered via gravitational perturbation by a companion, instabilities developing in the galactic disc or both. It has also been proposed that the so called "minor mergers", in which a gas rich galaxy and a satellite galaxy are involved could play an important role in triggering activity in Seyfert galaxies (de Robertis et al. 1998 and reference therein).

An efficient way to drag significant amount of mass in the central regions would be the presence of a large scale bar in the host galaxy, which could initiate strong inflows of gas (e.g. Athanassoula 1992; Friedli & Benz 1993). However, it has been shown in recent studies that if stellar formation is marginally enhanced in barred galaxies, the presence of an AGN is not correlated with the existence of a bar in its host galaxy (Mulchaey & Regan 1997; Ho et al. 1997). In fact, if the bar indeed initiates gas inflow, its inner Lindblad resonance (ILR), when present, stops the inflow and the gas is redistributed in a disc inside the ILR radius (e.g. Buta & Combes 1996). Thus a bar is clearly an efficient way to drag gas in the central regions (∼100 s pc), but another mechanism must take over to allow this gas to finally fall onto the AGN.

Shlosman et al. (1989) proposed that instabilities such as secondary bars could develop in the inner disc, starting again the gas inflow. During the past five years, a large

Send offprint requests to: E. Emsellem,
e-mail: emsellem@obs.univ-lyon1.fr

⋆ Based on observations collected at the VLT telescope of European Southern Observatory, Paranal, Chile, ESO Nos. 64.A-0076, 65.A-0031).

number of bars within bars have been detected and it becomes now possible to check statistically the impact of these structures on activity of galaxies. Whether or not there is a higher fraction of secondary embedded bars observed among Seyfert galaxies is still a matter of debate (Wozniak et al. 1995; Friedli et al. 1996; Jungwiert et al. 1997; Mulchaey & Regan 1997; Regan & Mulchaey 1999; Greusard et al. 2000). However, the lack of a clear correlation could be due to the different timescales in the involved processes (fuelling, AGN phase, bar dissolution). Still, bars within bars are often associated with bursts of star formation, confined within the nuclear bar, or the nuclear ring encircling it. Anyway, they do lead some significant evolution in the morphology and dynamics of the central regions of their hosts.

It is therefore important to trace both the dynamics and the stellar population of embedded bars, and examine potential links with the central AGN. So far, embedded bars have been observed essentially by optical or NIR imaging, whereas lack of collecting power has prevented any breakthrough from kinematic studies. Furthermore, if optical spectroscopy can be used to measure kinematics in dust-free regions, one has to move to less obscured wavelengths to map galaxy centres which are almost always very dusty (e.g. Valentijn 1990). As shown by Gaffney et al. (1995), the ^{12}CO absorption features at 2.29 μm, if not widely used, are a very efficient tool for measuring stellar kinematics in dusty environments. The age of the stellar populations can also be approached through the equivalent widths of these absorption ^{12}CO features (Doyon et al. 1994). Together with high-resolution NIR photometry, the kinematics can provide mass-to-light ratios, that also constrain the age of the populations.

We have thus undertaken a NIR spectroscopic study of a sample of Seyfert galaxies with and without double bars, using the spectrograph `ISAAC` mounted on the `VLT/ANTU`. The aim of this work, the `DEBCA` (Dynamics of Embedded Bars and the Connection with AGN) project, is to characterize the kinematics of stars and gas in the few 100 s inner parsecs, and to constrain the age of the stellar populations. We have so far obtained long-slit `ISAAC` spectroscopy of four Seyfert galaxies with double bars. In the present paper, the first of a series, we present the stellar kinematics extracted from these data, and discuss it in the light of simple dynamical models. A detailed discussion regarding the stellar populations is reported to a forthcoming paper (Greusard et al. 2001, in preparation, hereafter Paper II).

2. The DEBCA sample

The main goal of the `DEBCA` project is to study the link between the nuclear kinematics of the host galaxy and the fuelled central engine. We have thus compiled a list of single- and double-barred galaxies according to a few simple criteria:

- $-70^\circ < \delta < +20^\circ$ where δ is the declination of the target, for observations with the VLT;
- $30^\circ < i < 60^\circ$, where i is the inclination angle. This ensures that the bar is clearly visible, but with an inclination high enough to have significant velocity signatures;
- $D < 40$ Mpc, which constrains the minimum intrinsic physical scales ($0\farcs5 \sim 100$ pc) we can probe.

We have then selected a small sample of 12 galaxies, where both Seyfert 1 and 2 were required. Four of the targets are non-active galaxies, to be used as a "control sample". In the following Sections, we describe the observations and analysis of the first four targets of our list, three of them being generally classified as Seyfert 2's, and the fourth being a Seyfert 1 (Table 1). However evidence for the presence of a Seyfert nucleus in NGC 1808 is weak, this galaxy being better defined as a starburst galaxy: indeed optical and near-infrared spectra and more recent HST images strongly support the latter classification (e.g. Kotilainen et al. 1996). NGC 1097 and NGC 5728 are both classified as Seyfert 1's in the Veron-Cetty & Veron (1993) catalogue. Nevertheless, and although NGC 1097 does indeed contain an obscured broad-line region, characteristic of a hidden Seyfert 1 nucleus, the apparent nuclear activity of NGC 1097 is weak. This is also the case for NGC 5728 which was mentioned by Wilson et al. (1993) as a support for the unified model of Seyfert galaxies. We are therefore keeping NGC 1097 and NGC 5728 in the Seyfert 2 class.

3. The data

3.1. Observations

We obtained 12 hours of observing time in service mode (Period 63) and 2 nights in visitor mode (Period 64) at the `VLT/ANTU` with the `ISAAC` spectrograph. We have used the long-slit mode of `ISAAC` in its Short Wavelength configuration: characteristics are given in Table 2. Our spectral domain includes the first three or four (depending on the redshift of the galaxy) ^{12}CO bandheads, around 2.3 μm.

We defined Observing Blocks (`OB`) of 14 (`NDIT`) exposures of 180 s (`DIT`) each, operated in noding mode: the objects in exposures "A" and "B" were centred on the first and last third of the NIR array respectively. This (classical) procedure allowed us to have an excellent sky subtraction, using $A-B$ and $B-A$ differential exposures as working frames for the reduction.

We have observed 4 galaxies in our sample of 12, namely NGC 1097, NGC 1365, NGC 1808 and NGC 5728. Details for each galaxy are given in Table 3. Each galaxy was originally supposed to be observed for a total of 10 080 s (2.8 hours = 4 `OB`s). However, as mentioned in Table 3, we had to discard a number of exposures due to technical problems mainly due to:

- Spatial drifts of the slit during the `OB`;
- Slit jumps which resulted in a tilted slit both with respect to the NIR array and the noding.

We also observed a set of stellar kinematical templates (typically G, K and M giants) to be used for the

Table 1. Optical data for the 4 galaxies

Galaxy	D [Mpc]	M_B [mag]	Diameter [′ × ′]	Sey	Bar[1]	Type	$V_{\rm sys}^{\rm Leda}$ [km s^{-1}]	$V_{\rm sys}^{\rm obs}$ [km s^{-1}]	PA$_{\rm disc}$ [◦]	i [◦]	PA$^2_{\rm pb}$ [◦]	PA$^3_{\rm nb}$ [◦]
NGC 1097	16.8	10.2	9.3 × 6.3	S2	DB	SBb	1273	1240	130	37	138	30
NGC 1365	18.6	10.3	11.2 × 6.2	S1	DB	SBb	1653	1628	32	57	91	45
NGC 1808	10.9	10.8	6.5 × 3.9	SB⋆	DB	SABb	1003	1015	133	70	143	157
NGC 5728	37.0	12.4	3.1 × 1.8	S2	DB	SABa	2789	2836	30	55	33	79

[1] DB means Double Bar.
[2] PA of the Primary Bar.
[3] PA of the Nuclear Bar.
⋆ Starburst galaxy: evidence for a Seyfert nucleus in NGC 1808 is weak, see text.

Table 2. Instrumental setup of `ISAAC`

`ISAAC` SW mode	
Slit	$0\farcs6 \times 120''$
Spatial sampling	$0\farcs147$
Spectral sampling	1.19 Å
Spectral resolution	4478
Spectral $FWHM$	67 km s^{-1}
Wavelength interval	1200 Å centred at 2.336 μm

Table 3. DEBCA-`ISAAC` data characteristics. The observation period is given in column "P". Numbers of OBs are indicated as used/discarded respectively. "Exp" is the total exposure time on target. $FWHM_\star$ corresponds to the mean seeing. The orientation of each slit with respect to the nuclear bar major-axis is given in Col. 3, the PA of the slit is given in Col. 4

Galaxy	P	axis	PA [°]	# OB	Exp. [min]	$FWHM_\star$ [″]
NGC 1097	63	//	29.5	4 / 0	168	0.8
		⊥	119.5	5 / 0	168	0.7
NGC 5728	63	//	264.5	4 / 0	168	0.6
		⊥	354.5	4 / 0	162	1.5
NGC 1365	64	//	45.5	4 / 0	162	1.0
		⊥	135.4	4 / 1	162	1.0
NGC 1808	64	//	335.5	5 / 0	210	0.7
		⊥	65.5	3 / 2	112	0.6

kinematical measurements, and solar type stars for the correction of telluric features (see Maiolino et al. 1996).

In our spectral domain, there are no OH lines, generally useful to perform a wavelength calibration of the exposures. We had thus to rely on independent arc lamp exposures to perform our wavelength calibration. In this context, we asked individual arc exposures *during the night*.

3.2. Data reduction

In the following paragraphs, we give a brief description of the reduction and analysis procedure we applied to our data. We emphasize some of the problems we encountered on the way, most of them linked with instrumental issues (all data were taken prior to the major overhaul in Feb. 2000). All the reduction processes were applied using the `IRAF` and `MIDAS` packages, as well as a few low level routines from the `Eclipse` package.

Since we observed in nodding mode, we used the differential comparison ($A - B$ and $B - A$) to subtract the dark, bias and sky contribution from all exposures. The data were then flat-fielded using a previously prepared master flat field image: variations of up to 5% were measured on the flat fields during a night. We then corrected for the distortion along and perpendicular to the slit, using the star-trace exposures provided by ESO, and associated arc lamps. Systematic residual (low frequency) distortion were of the order of 0.2–0.3 pixel, not fully satisfactory, but sufficient in the context of our program. It seems that these residuals cannot be further damped, as the distortion pattern varied on a medium time range at the time of the observations (which means that the star-trace exposures were not stable enough).

The data were then wavelength calibrated. As already mentioned, there are no sufficiently bright OH lines in our spectral domain to allow any spectral calibration, and we had to rely on independent arc lamp exposures. Unfortunately, at the time of the observations, there was a (known) problem with the dispersor which seems to shift from one `OB` to the next, following an automatic software initialisation. We have indeed observed some significant shifts (typically a few tenths of a pixel) along the dispersion direction between successive `OB`s. This is critical for our program as we are looking for a velocity accuracy of <5 km s^{-1}, a third of a pixel. This problem was solved by using sky emission lines to correct for any residual zeroth order shift.

Individual exposures are then combined, after careful recentring, and corrected for telluric absorption using a solar type stellar template as described in Maiolino et al. (1996), and taking into account the difference in line depth (depending on e.g. the differential airmass). The result is illustrated in Fig. 1 for a K0III star. The present data reduction only provided us with a relative flux calibration, sufficient for kinematical purposes.

3.3. Kinematical analysis

The (stellar template and galaxy) spectra were finally rebinned in $\ln(\lambda)$ to be sampled with constant bins in

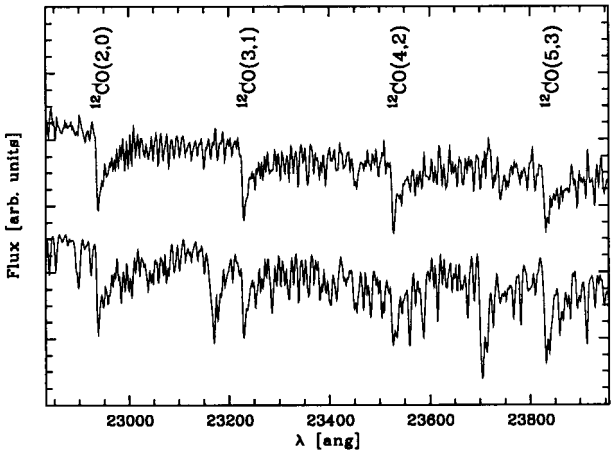

Fig. 1. ISAAC (aperture) spectrum of HD 16492, a K0 giant, before (bottom) and after (top) correction for the telluric absorption. The main ^{12}CO lines are identified

velocity space. We first binned spectrally by a factor of 2 as this leads to a pixel of about 31 km s^{-1}, properly sampling the original spectral resolution of the data (see Table 2). We also binned the data spatially along the slit to ensure a minimum signal to noise ratio of 20, required to extract the stellar kinematics. We then performed a continuum subtraction using a low order polynomial. A refined version of the Fourier Correlation Quotient (Bender 1990) was used to derive the line-of-sight velocity distribution and to measure the first two velocity moments (V and σ): we used different templates and checked that the resulting kinematics were not significantly affected by template mismatching. Measurements of higher order Gauss-Hermite moments will wait for the building of optimal templates (Paper II). The central velocity value was assumed to be the systemic velocity and subtracted from each individual velocity profile[1].

We derived formal errors for the kinematics using a Monte Carlo approach. Fixing the signal to noise ratio and the velocity dispersion, we made 500 realisations of simulated broadened spectra, measured the kinematics via FCQ, and derived the resulting standard deviation for V and σ, S_V and S_σ respectively. S_V and S_σ were tabulated for 5 values of σ and 40 values of the signal to noise. We then derived the errors for individual data points via interpolation.

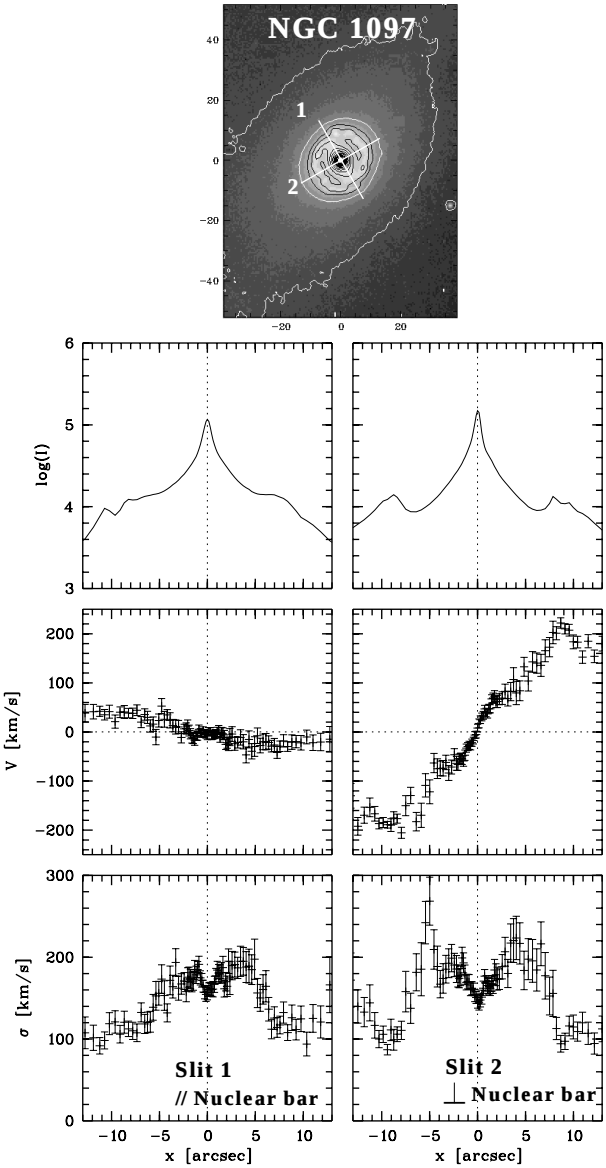

Fig. 2. Kinematical profiles of NGC 1097. From top to bottom: NIR image of the galaxy centre (North is up, East is left), indicating the positions and lengths of the two slits, parallel and perpendicular to the nuclear bar (the labels 1 and 2 overimposed on the image indicate positive abscissa); luminosity profiles (in log) along the two slits; velocity and dispersion profiles with error bars representing $3 \cdot S_V$ and $3 \cdot S_\sigma$ values (see Sect. 3.3)

4. Kinematical results

The kinematical profiles obtained for the four galaxies are displayed in Figs. 2–4 and 6. In each figure, the lengths of the sketched slits overimposed on the image correspond to the presented profiles.

For the interpretation of the velocity profiles, it is important to keep in mind that the spectra have been taken along slits parallel and perpendicular to the nuclear bars (respectively named Slit 1 and Slit 2 hereafter). The major and minor axis of the galaxies do not coincide with that of the bars, so that we do expect some rotation along both axis, due to the inclination effect. The various position angles and inclinations are displayed in Table 1.

4.1. Individual descriptions

NGC 1097, Seyfert 2, $1'' \sim 81$ pc: The luminosity profile along Slit 1 falls down to a plateau near the end of

[1] Systemic velocities derived from the minor and major axis of a galaxy were always found to be consistent with each other, within the error bars.

the nuclear bar, and then decreases longward $\sim 10''$ with a roughly exponential law characteristic of a disc population. This is fully consistent with the $10.3''$ semi-major axis extent of the nuclear bar mesured by Friedli et al. (1996). The luminosity along Slit 2 follows the same behaviour, but with a bump just after the plateau due to its well–known circumnuclear clumpy ring (actually a tightly wound spiral structure in the NIR; e.g. Kotilainen et al. 2000).

The velocity profile along Slit 1 is quite flat, reflecting the fact that it is nearly perpendicular to the kinematical line of nodes (which we assume to be given by the major-axis photometric position angle of the outer disc of the galaxy). The global shape of the rotation curve along Slit 2 roughly resembles the Hα velocity curve derived (along a position angle of 130°) by Storchi-Bergmann et al. (1996). The maximum stellar velocity along Slit 2 ($V_{\rm max,2} \sim 210\,{\rm km\,s^{-1}}$) is reached in the circumnuclear ring, similarly to the ionised gas for which Storchi-Bergmann et al. (1996) measures maxima of $V_{\rm max}[{\rm H}\alpha] \sim 225\,{\rm km\,s^{-1}}$. We thus measure a roughly constant stellar velocity gradient of $\sim 290\,{\rm km\,s^{-1}\,kpc^{-1}}$. Our good spatial resolution however allows to reveal a richer velocity structure. Inside $R = 5''$, the velocity profile along Slit 2 exhibits an S-shape with nearly flat ends. Those plateaus in the velocity correspond to maxima in the dispersion profile ($\sigma_2 \sim 220\,{\rm km\,s^{-1}}$), whereas the inner part is characterised by a quite surprising drop in the dispersion (down to $\sigma_2 \sim 145\,{\rm km\,s^{-1}}$ at the centre). Velocities increase almost linearly from a radius of $5''$ reaching a maximum near the edge of the circumnuclear ring at $\sim 9''$, where they then starts to decrease. Outside $5''$, the dispersion decreases outwards down to $\sim 95\,{\rm km\,s^{-1}}$. Note that the dispersion drop and local maxima in the dispersion are also present along Slit 1.

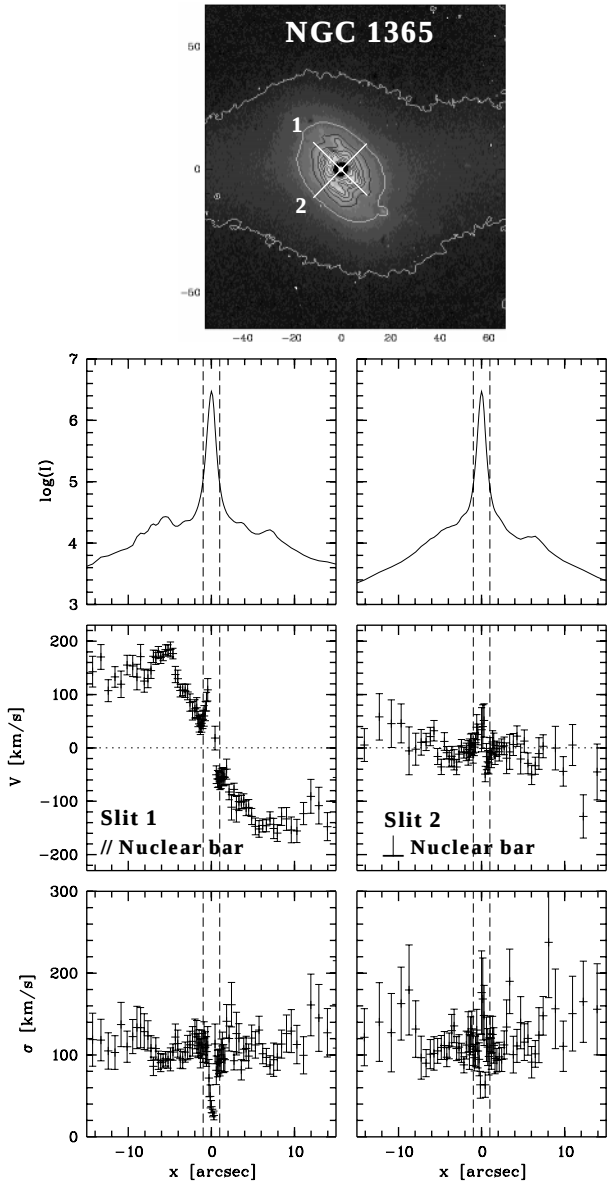

Fig. 3. Same as Fig. 2 for NGC 1365. The light in the central arcsecond (region marked by the vertical dashed lines) is completely dominated by the non-thermal contribution of the Seyfert 1 nucleus, thus preventing us to derive any meaningful kinematics in this region

NGC 1365, Seyfert 1, $1'' \sim 90$ pc: The Seyfert 1 nucleus of NGC 1365 dominates the light in the central arcsecond, and thus strongly dilutes the absorption ^{12}CO bandhead: this prevented us to derive any meaningful kinematics in this region. We will deal here only with the profiles outward $R \geq 2''$.

Like in NGC 1097, the flatness of the velocity profile along Slit 2 is a consequence of the slit orientation with respect to the line of nodes. The central kpc morphology of this galaxy is disturbed by an intense star formation (see Lindblad 1999 for a review on this object). It is thus difficult to see the signature of the bar in the luminosity profile. Ellipse fitting on H-band isophotes provided by Jungwiert et al. (1997) gave a rough estimate of the extent of the presumed secondary bar: $\sim 9 - 10''$. However, high resolution near-infrared images of the central region of NGC 1365 recently obtained with NICMOS/HST, and the VLT (ISAAC and FORS1) suggest that the ellipticity of the component detected in the central $10''$ is solely due to the inclination of the galaxy (the photometric major-axis being thus coincident with the line of nodes). There are therefore no evidence left for the presence of a nuclear bar. We then simply interpret the observed flattened system in the centre as a nuclear disc, well circumvented by a ring-like (and spiral arm) structure at a radius of $\sim 7''$. Inside this radius, the velocity increases up to its maximum value ($V_{\rm max,1} \sim 175\,{\rm km\,s^{-1}}$ at $R \sim 5''$) with a steep gradient ($\sim 390\,{\rm km\,s^{-1}\,kpc^{-1}}$), and then remains roughly constant until the end of the disc. The dispersion along both axis shows no clear structure: it remains nearly constant inside the nuclear disc with a mean $\sigma_1 \sim 100\,{\rm km\,s^{-1}}$. There may be a slight increase outwards up to $\sigma_2 \sim 120 - 130\,{\rm km\,s^{-1}}$, but this is within the error bars.

NGC 1808, Seyfert 2, $1'' \sim 53$ pc: The central kpc of this galaxy, disturbed by "hot spots" of star formation (e.g. Kotilainen et al. 1996), is the brightest of our sample

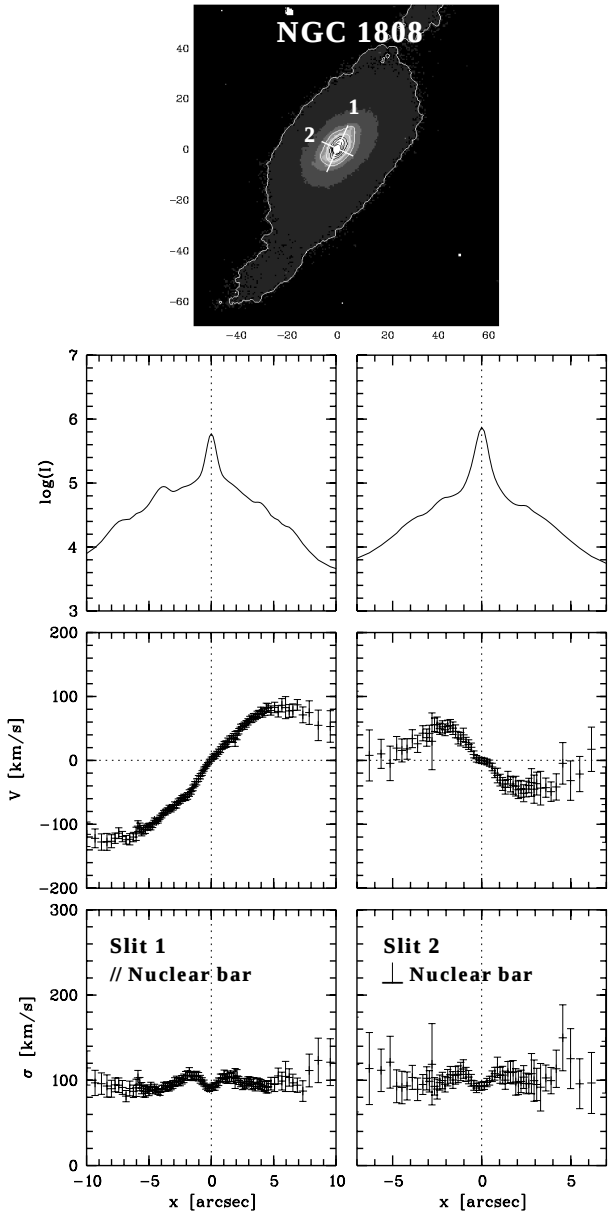

Fig. 4. Same as Fig. 2 for NGC 1808

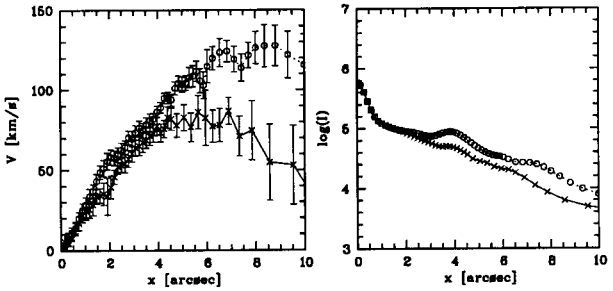

Fig. 5. Velocity (left, absolute values) and surface brightness (right) profiles along Slit 1 of NGC 1808: the crosses and solid lines correspond to the north–west side, the circles and dotted lines to the south-east side

in the K-band, hence providing the nicest kinematic profiles. Again, we estimate the nuclear bar length to be $\sim 6''$ from Jungwiert et al. (1997), with an axis ratio around 0.5. The velocity profiles along both axis show an increase up to the end of the nuclear bar and then a decrease. Slit 1 velocity profile is significantly asymmetric with respect to the systemic velocity outside $2''$, with $V_{\rm min,1} = -124$ km s^{-1} and $V_{\rm max,1} = 81$ km s^{-1}: this asymmetry is also clearly present in the surface brighness profile (Fig. 5) but does not appear in the dispersion curve. Along Slit 2, the velocity profile is roughly symmetric with local extrema $V_{\rm min,2} \sim -45$ km s^{-1} and $V_{\rm max,2} \sim 53$ km s^{-1} at radii of $\pm 2''$, followed by a decrease outwards down to systemic velocity. The mean slopes in the rising parts are $\sim$300 km s^{-1} kpc^{-1} and 260 km s^{-1} kpc^{-1} along Slit 1 and Slit 2 respectively. There is however a distinct kink in the velocity profile along Slit 1 at a radius of $-2''$, with no symmetric counterpart. The velocity gradient changes inside $0\farcs4$ of Slit 2, to only $\sim$140 km s^{-1} kpc^{-1}, a real feature considering the final spatial resolution for this slit ($\sim 0\farcs6$ $FWHM$; see Table 3). The dispersion profiles remain in the range 80–120 km s^{-1}and exhibit a trend similar to the one of NGC 1097: an increase toward the centre followed by a significant drop this time inside $1''$. The magnitude of this drop is low ($\sim$15 km s^{-1}) but real.

NGC 5728, Seyfert 2, $1'' \sim 179$ pc: NGC 5728 is the faintest galaxy in our sample, however the signal-to-noise is enough to have a good measure of the velocity profiles in the central $5''$. Once again, there are clear signatures of a decoupled dynamical component in the central kinematics. The maximum velocity gradient is observed along Slit 2 as expected from the position angle of the line of nodes (see Table 1), similarly to the case of NGC 1097. Slit 1 for NGC 5728 is very close to the slit used by Prada & Gutierrez (1999, hereafter PG99; PA = 86°), our velocity profile being consistent with theirs. The velocity and velocity dispersion profiles are slightly asymmetric along both slits. The K band surface brightness profile also exhibits an asymmetry along Slit 1 at the edge of the nuclear bar. There is a dip in the dispersion profiles of NGC 5728, with a central value of 147 km s^{-1}, although it is less convincing than in the cases of NGC 1097 and NGC 1808. This value is slightly smaller than but within the error bar of the one derived by PG99. We do not detect any double component in our LOSVDs, in apparent contradiction with the data of PG99. We observe a high excitation [CaVIII] emission line, burried within the second ^{12}CO absorption feature. The emitting region is restricted to the central spectra, and is consistent with an unresolved point-like source, thus certainly linked with the AGN. This point will be examined in details in a forthcoming paper (Paper II).

4.2. Global results

The first striking result of those observations is that, in all 4 observed targets, the rotational velocity reveals a maximum inside the nuclear bar (or disc for NGC 1365) and

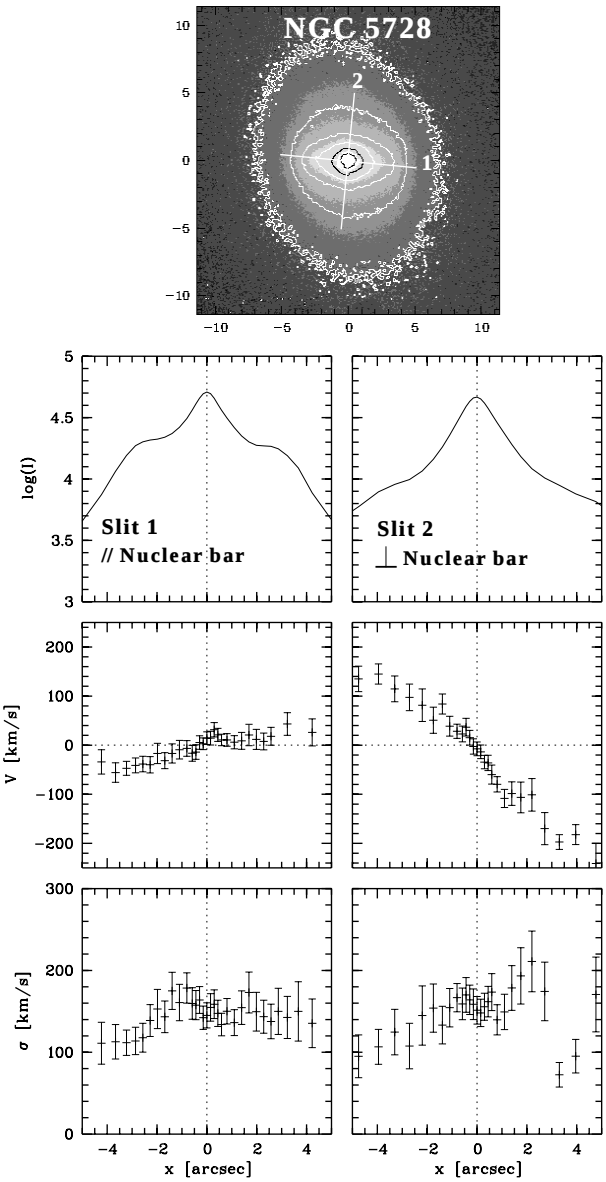

Fig. 6. Same as Fig. 2 for NGC 5728. Note the different spatial extent of the major and minor axis plots

then decreases[2], showing that the nuclear region is a well decoupled dynamical component of the galaxies. For the three cases with nuclear bars (NGC 1097, NGC 1808 and NGC 5728), this follows suggestions made from photometric studies as no preferential angle was observed between the two bars (Greusard et al. 2000 and references therein). The existence of such structures could be doubted when dealing with a galaxy like NGC 1808, where there are numerous clumps of star forming systems within the central arcseconds. But even in that case, the NIR photometric elongation embedded within the ring present in the WFPC2/HST (archival) images strongly suggests the presence of a nuclear bar. This point is further examined in the light of dynamical models (Sect. 5). This is therefore the first direct confirmation of the dynamically decoupled nature of nuclear bars.

The second surprising result comes from the dispersion profiles: they exhibit a significant drop at the centre (but again we cannot say anything concerning NGC 1365). This is particularly clear in the cases of NGC 1097 and NGC 1808. We have checked that the dilution of the lines by any featureless continuum component does not affect the dispersion (and velocity) as long as the ^{12}CO lines remain strong enough. We do indeed see some dilution and changes in the ^{12}CO line strength, but this does not affect our result. We have also checked that the observed central dispersion drop is not due to a template mismatching effect (Paper II).

5. Modelisation of the kinematics

For each galaxy, we wish to reconstruct the entire velocity field, projected on the sky, and constrain it with the observed velocity profiles along the short and long axis of the nuclear bar (or disc for NGC 1365). Three of the four galaxies observed here have embedded nuclear bars, and the orbits are then not expected to be circular. To interpret these profiles, in a first approximation, we build simple models of the orbital structure, based on the epicyclic theory, assuming that the departures from circular motions are small.

5.1. Linear approximation

We introduce the usual coordinate system (ξ, η), rotating with the angular speed of rotation $\Omega - \Omega_{\rm p}$ in the frame co-rotating with the bar perturbation ($\Omega_{\rm p}$).

$$r = r_0 + \xi$$

$$\theta = \theta_0 + (\Omega - \Omega_{\rm p})t + \eta/r_0$$

where θ is the azimuthal angle in the rotating frame.

The bar potential is modelled by the function:

$$\Phi(r, \theta) = -\Phi_2(r)\cos 2\theta + ...$$

with small harmonic terms ($\Phi_4, \Phi_6 \leq \Phi_2$). The shape of the bar potential is taken from the $k = 3$ bar of the surface density-potential pairs generated by Kalnajs (1976):

$$\Phi_2(r) = 0.53 q_{\rm bar} x(1. - 2.5x + 2.1875x^2 - 0.65625x^3)$$

when $x = r^2/r_{\rm bar}^2 < 1$. Outside $r_{\rm bar}$, the potential is extrapolated by continuity, with an inverse power law (in r^{-4}). The strengths of the bars $q_{\rm bar}$ are chosen such that the perturbations in the velocity field match at best the data. The strength of the perturbation is best quantified by the maximum over the disc of the ratio of the tangential force to the radial force, $P2_{\rm max}$. This quantity is given in Table 4 for the four galaxies.

The equations of motion are linearized; in order to take into account the transition at the inner Lindblad resonances, an artificial frictional force is introduced, with a

[2] In the case of NGC 5728, we hardly reach the end of the nuclear bar so that the velocity decrease is less obvious, but see PG99.

damping coefficient λ, as is usually done to simulate gas orbits (Lindblad & Lindblad 1994; Wada 1994). The motion is that of an harmonic oscillator, forced by an imposed external perturbation. The equations can be solved, at the neighborhood of the ILR (and OLR) and far from corotation, and give the coordinates and velocities of the orbit of the guiding centre, the epicyclic motions around this centre being damped by the frictional force.

This formulation (see Appendix A) accounts for the change of orientation of orbits at the crossing of resonances (parallel or perpendicular to the bar), and when the damping parameter λ is not zero, of a gradual orientation change, corresponding to the gas spiral arms. We also use models with spiral configurations, since some young supergiant stars, just formed out of the gas, share its dynamics (and are indeed observed in the NIR range).

5.2. Galaxy models

The mass model for the spiral galaxies is made of three components:

- a small bulge, of Plummer shape potential

  $$\Phi_{\rm b}(r) = -\frac{GM_{\rm b}}{\sqrt{r^2 + r_{\rm b}^2}}$$

  with characteristic mass $M_{\rm b}$ and radius $r_{\rm b}$;
- a Toomre disc, representing the main stellar disc, of surface density

  $$\Sigma(r) = \Sigma_0 (1 + r^2/r_{\rm d}^2)^{-3/2}$$

  truncated at $r_{\rm t}$;
- a nuclear disc, which corresponds to the decoupled nuclear bar, and is required to account for the large gradients of velocity profiles, observed at kpc scale in the present work. Its shape is also taken as a Toomre function:

  $$\Sigma(r) = \Sigma_0 (1 + r^2/r_{\rm nd}^2)^{-3/2}$$

  with a characteristic mass $M_{\rm nd}$ and radius $r_{\rm nd}$.

Let us emphasize that within the centre of spiral galaxies, the presence of dark matter is not required (e.g. Freeman 1992): the spherical dark matter halo, usually added to flatten rotation curves at large radii, have such a large characteristic radius that it has no influence on the inner parts considered here. All parameters are displayed in Table 4. From these analytical components, it is easy to compute the critical velocity dispersion for axisymmetric instability at each radius. We assume that the radial velocity dispersion $\sigma_{\rm r}$ is everywhere proportional to this critical velocity, with a constant Toomre parameter Q as a function of radius. The value of Q is also indicated in Table 4. The tangential velocity dispersion σ_θ is assumed to verify the epicyclic relation:

$$\sigma_\theta = \frac{\kappa}{2\Omega}\sigma_{\rm r}.$$

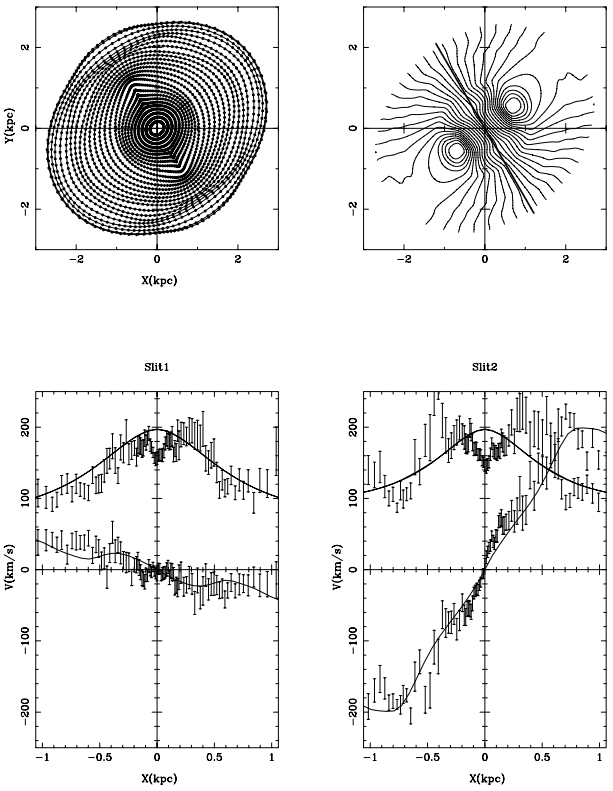

Fig. 7. Model velocity profiles for NGC 1097. Top left: the shape of the orbits in the linear epicyclic approximation, projected on the sky plane. Top right: the deduced velocity field, with the orientation of the nuclear bar indicated. Bottom: The corresponding velocity profiles, along the nuclear bar (left), and perpendicular to it (right) overimposed on the ISAAC kinematical profiles and their corresponding error bars. Two lines are plotted for the modeled velocity dispersion profiles, including or not the velocity gradients in the resolution elements. Most of the time, the two profiles are coinciding

The disc plane is assumed to have a constant scale-height h_z with radius, and the z-velocity dispersion is derived from the surface density in the disc $\Sigma(r)$ by:

$$\sigma_z^2(r) = 2\pi G \Sigma(r) h_z.$$

For each observed slit, we have computed the velocity dispersion along the line-of-sight in combining the local dispersion, and the contribution of the velocity gradient in the observed spatial resolution. Even in the very centre of the galaxies, this second contribution was always negligible.

5.3. Fits of the observations

The results of the modelisation can be seen in Figs. 7–10 for the four galaxies. In all cases, the presence of the nuclear disc is necessary to account for the large velocities at the kpc scale. The small bulges allowed by the photometry are insufficient, and in general bring a negligible contribution to the rotation curve. To limit the number of free parameters, we have fixed the mass and radius of the bulges to the statistical relation found by de Jong (1996) through

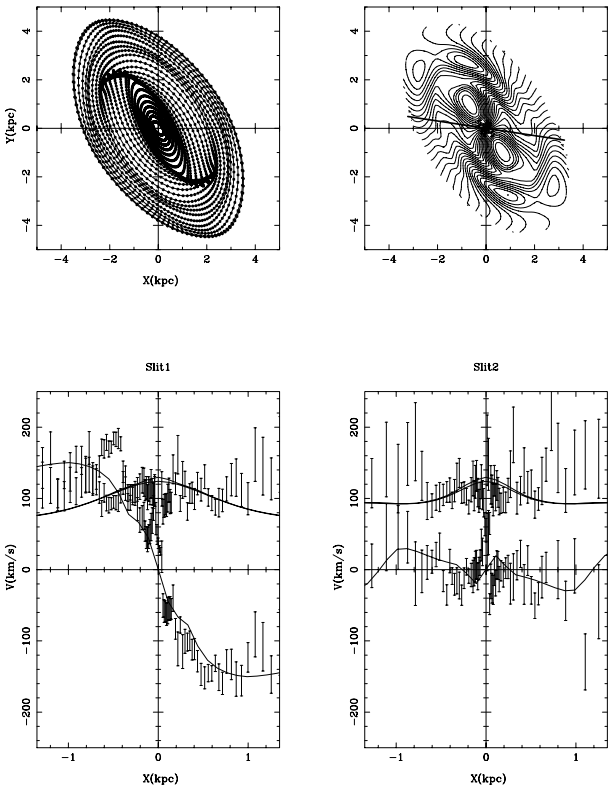

Fig. 8. Model velocity profiles for NGC 1365. (See Fig. 7 for caption)

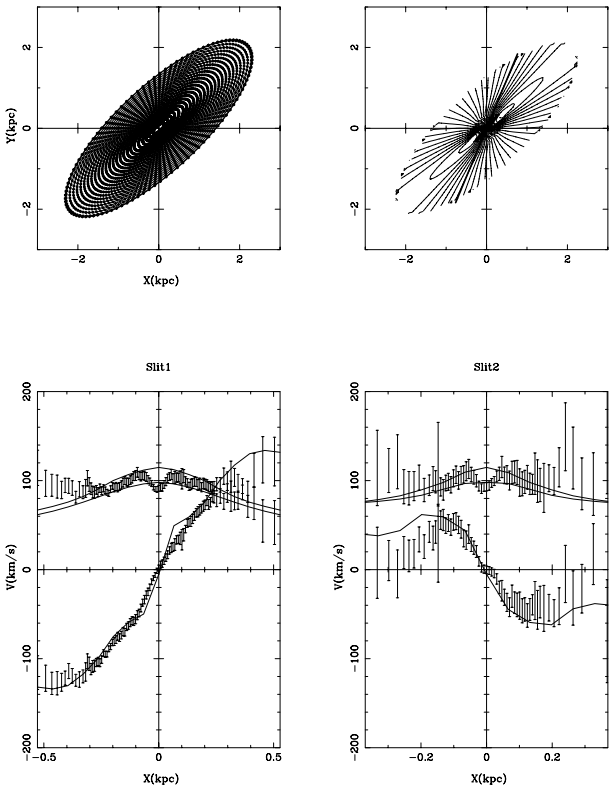

Fig. 9. Model velocity profiles for NGC 1808. (See Fig. 7 for caption)

NIR photometry. According to the types of the present galaxies, the bulge-to-disc ratio is 0.1, and the bulge radius is about 10 times lower than the disc radius. The main stellar disc are truncated at $r_{\rm disc} = R_{25}$, and their radial scale-lengths are deduced, assuming a central surface brightness of 21 B-mag arcsec^{-2}. The scale-heights of the discs are chosen to be 0.2 times the radial scale-length (e.g. Bottema 1993). The remaining free parameters to fit are therefore:

- $M_{\rm d}$ the disc mass, which is constrained by the outer parts of the velocity curve;
- $M_{\rm nd}$ and $r_{\rm nd}$ the mass and characteristic size of the circumnuclear disc. These parameters are constrained by the inner parts of the rotation curve;
- The strength and radius of the bar, $q_{\rm bar}$ (or equivalently $P2_{\rm max}$) and $r_{\rm bar}$, together with the pattern speed $\Omega_{\rm p}$, constrained by the shape and amplitude of the velocity profile;
- Q the Toomre parameter, constrained by the observed dispersion.

Since we are concerned here only with the circumnuclear regions, there is no corotation inside the model, but most of the time the best fit of $\Omega_{\rm p}$ is such that there are one or two inner Lindblad resonances.

For all galaxies except NGC 1365, the best fit is obtained with a nuclear bar, oriented differently than the primary bar, and parallel to the apparent nuclear bar. For NGC 1365 however, it was better to keep the primary bar potential orientation, with its low pattern speed, and rely on the different phase orientation of the orbits, to form a spiral nuclear structure, between the two ILRs. This confirms the observation that NGC 1365 does not include a secondary bar, as previously claimed, but a decoupled nuclear disc surrounded by spiral arms within the ILR of the primary bar.

In no case was it possible to find any central drop for the velocity dispersion. Of course, there is still a certain latitude in the fitting procedure, but some features are certain: it is not possible to reproduce the observations without a circumnuclear disc component, or with an axisymmetric potential. Elliptical orbits are required, and the fits give an order of magnitude of their importance. Also the required mass of the circumnuclear disc component is comparable, and sometimes even greater, than the bulge mass. The present models are simple first approximations, with bi-symmetry imposed (there is no $m = 1$ components, although in NGC 1808, such an asymmetry is clearly observed); more realistic models constrained by further detailed kinematical data are needed to precise the dynamics of the double-bar galaxies. New models will also help to examine the issue of the central mass concentrations, for which we cannot, at the moment, give a lower limit.

Table 4. Model parameters for the 4 galaxies

Galaxy	$M_{\rm b}$ 10^{10} $M_\odot$	$r_{\rm b}$ kpc	$M_{\rm nd}$ 10^{10} $M_\odot$	$r_{\rm nd}$ kpc	$M_{\rm d}$ 10^{10} $M_\odot$	$r_{\rm d}$ kpc	$r_{\rm t}$ kpc	Q	h_z kpc	$r_{\rm bar}$ kpc	$\Omega_{\rm p}$ km s^{-1}/kpc	$P2_{\rm max}$
NGC 1097	1.3	0.6	1.6	0.9	13	5.9	22	1.5	1.2	3	78	0.06
NGC 1365	1.0	0.8	1.1	1.2	10	8.0	30	1.8	1.6	5	25	0.23
NGC 1808	0.3	0.3	0.9	0.4	2.7	2.7	10	1.4	0.5	0.9	60	0.07
NGC 5728	0.4	0.4	0.9	0.6	3.8	4.3	16	1.6	0.9	3	50	0.06

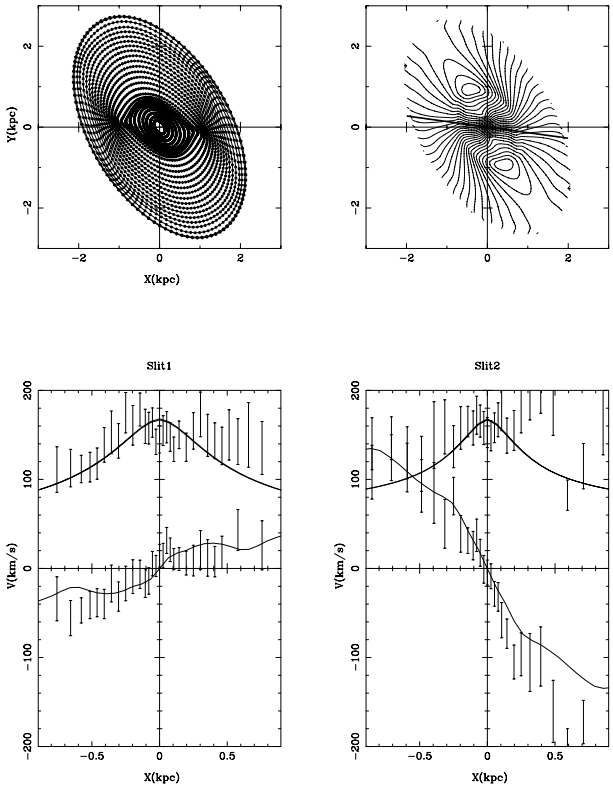

Fig. 10. Model velocity profiles for NGC 5728. (See Fig. 7 for caption)

6. Discussion and conclusions

We have presented the stellar kinematics of 4 galaxies hosting an active nucleus, namely NGC 1097, NGC 1365, NGC 1808 and NGC 5728, derived from ISAAC/VLT spectroscopy at 2.3 μm.

The essential results regarding the stellar kinematics of the nuclear bars are the confirmation of the decoupling of the nuclear component (with respect to the primary disc and bar), and the discovery of a central velocity dispersion drop in at least 3 targets out of 4 (being unable to derive the central kinematics for NGC 1365 due to the contribution of its Seyfert 1 nucleus). The observed central dispersion dips are not significantly affected when optimal templates are used to derive the kinematics (Paper II): it is therefore a robust result. We also observed a strong asymmetry in the stellar velocity profiles of NGC 1808, following the asymmetry in the photometry, and suggesting the existence of an $m = 1$ mode in the central region of this galaxy. The detailed discussion of the double-bar dynamics is postponed to forthcoming papers, where it will be interpreted in terms of numerical simulations (through hydrodynamical N-body simulations and through determination of the orbital families with the Schwarzschild's method). In the following, we will discuss possible interpretations for the observed velocity dispersion drops.

The observation of a velocity dispersion drop at the centre of spiral galaxies is rare. Such a drop has been observed in NGC 6503 by Bottema (1989), where the dispersion decreases within the central 12″. The phenomenon could be more widespread at smaller radii, as it would be difficult to recognize it with limited spatial resolution. In NGC 1097, the dip extends only 4″ in radius, about 1.″5 in NGC 1808, and 1″ in the case of NGC 5728. The physical extent of the dispersion drop in NGC 1097 (radius of $\sim$4″ $\equiv$ 325 pc at 16.8 Mpc) is comparable to the one of NGC 6503 ($\sim$12″ $\equiv$ 350 pc at 6 Mpc), but significantly larger than the ones in NGC 5728 ($\sim$1″ $\equiv$ 180 pc at 37 Mpc) and in NGC 1808 ($\sim$1.″5 $\equiv$ 80 pc at 10.9 Mpc).

Bottema (1993) made a compilation of the velocity dispersion profiles of a dozen spiral galaxies, and only NGC 6503 exhibits this drop. In general, the dispersion profile is well fitted by an exponential law, decreasing with a characteristic scale of twice the photometric scalelength for the disc. When the bulge is significant, the fit is compatible with a constant dispersion for the bulge. This exponential law for the disc is naturally explained for face-on galaxies, i.e. for the vertical velocity dispersion profiles. Indeed, it has been shown by van der Kruit & Searle (1981, 1982) that the galactic discs have a constant scale-height with radius. Since the surface density in the plane has an exponential distribution (Freeman 1970), the vertical equilibrium of a self-gravitating disc implies that the dispersion varies as the square root of the surface density, therefore in $e^{\frac{-r}{2h}}$, where h is the disc radial scalelength. If the ratio between the radial and vertical dispersions is maintained constant with radius, this will also imply the same exponential behaviour for the in-plane dispersion. Observations of the velocity profiles in inclined galaxies seem to support this hypothesis of a constant ratio (Bottema 1993).

Also an interpretation in terms of disc stability and self-regulation with the Toomre Q parameter has been advanced (Bottema 1993). Stars are heated by gravitational instabilities like spirals and bars. When the Q parameter is too small, instabilities set in, until the velocity dispersion has increased up to the threshold Q. The gaseous component allows a much richer feedback regulation, since it can cool down through dissipation and provoke recurrent

instabilities. Young stars are formed out of the gas with relatively low velocity dispersion. It is easy to see how gravitational instabilities could lead to a constant Q value all over the stellar discs.

Bottema & Gerritsen (1997) have re-examined the problem of the dispersion drop in the centre of NGC 6503, and find no intrinsic explanation. An hypothesis is to assume a very thin and cold disc in the centre, but it is difficult to avoid heating of this disc through gravitational instabilities. They have undertaken N-body simulations to check the stability of such a disc, and found only negative results: no dispersion drop was ever observed in the simulations, whatever the initial conditions. They conclude that the only solution is to assume the existence of an independent system in the nucleus, a different population, that could have been recently accreted from outside. The accretion must be quite recent. Another explanation is the existence of two counter-rotating bars, as suggested by Friedli (1996). This hypothesis is not supported by the observed kinematics in any of the three cases studied in the present paper.

It could also be considered that fresh gas is radially falling inwards, because of gravitational torques from a bar for instance, and that this gas is piling up in a thin disc in the centre, then forming new stars with a low velocity dispersion. There should have been then a recent starburst in the centre of the galaxy. This scenario is likely for NGC 1808, as we indeed detect a young stellar component in its centre (Paper II). The case of NGC 1097 may be more difficult to assess. Kotilainen et al. (2000) did find some recent (6–7 Myr ago) star formation in the central region of NGC 1097, but well distributed along its well-known (ILR) ring-like structure. There is no evidence so far for a recent starburst inside the ring, although we can not discard this hypothesis. New self-consistent N-body simulations including star formation however support this scenario as an explanation for the observed central dispersion drop (Wozniak et al. 2001, in preparation). We still need to understand how common this phenomenon is, among galaxies with and without bars (single or double), and how it is linked to the nuclear activity.

Appendix A: Formulae in the linear approximation

In the absence of a non-axisymmetric perturbation, the orbits can be computed in the epicyclic approximation, and the variables ξ, $\eta << r_0$ follow the evolution of an harmonic oscillator, with the epicyclic frequency κ. In the presence of a bar perturbation, the equations of motions, in the reference frame rotating with the perturbation at $\Omega_{\rm p}$ are (Lindblad & Lindblad 1994):

$$\ddot{\xi} - 2\Omega\dot{\eta} - 4\Omega A\xi = \frac{\mathrm{d}\Phi_2}{\mathrm{d}r}\cos 2\theta = C\cos 2\theta$$

$$\ddot{\eta} + 2\Omega\dot{\xi} = -2\frac{\Phi_2}{r}\sin 2\theta = -D\sin 2\theta$$

where A is the Oort constant:

$$A = -\frac{1}{2}r\frac{\mathrm{d}\Omega}{\mathrm{d}r},$$

related to the epicyclic frequency κ by:

$$\kappa^2 = 4\Omega^2 - 4\Omega A.$$

The oscillator is now forced by an external perturbation at the imposed frequency $\omega = 2(\Omega - \Omega_{\rm p})$.

Taking for ξ and η a solution of the form:

$$\xi = a\cos(2\theta + 2\psi) + c\,\mathrm{e}^{-\lambda t}\cos(\kappa' t + \phi_0)$$

$$\eta = b\sin(2\theta + 2\psi) + c'\,\mathrm{e}^{-\lambda t}\cos(\kappa' t + \phi_0)$$

with the same phase angle ψ (ξ and η in quadrature), and κ' the modified proper frequency of the damped oscillations, it can be found that:

$$a = \frac{\frac{\mathrm{d}\Phi_2}{\mathrm{d}r} + 4\frac{\Omega}{\omega}\frac{\Phi_2}{r}}{\sqrt{(\kappa^2 - \omega^2)^2 + 4\omega^2\lambda^2}}$$

and

$$\tan 2\psi = -\frac{2\omega\lambda}{\kappa^2 - \omega^2}$$

with

$$\omega^2 b = D - 2\Omega\omega a.$$

The damped terms, exponentially decreasing with λt, correspond to the epicycles around the guiding centers, and are not considered here (only through the velocity dispersion).

Acknowledgements. We wish to thank Jean-Gabriel Cuby and Claire Moutou for their help and support during the ISAAC observations. We also wish to thank the referee, Alan Morwood, for a detailed and critical reading of the manuscript. This work has been supported by the Swiss National Science Foundation.

References

Athanassoula, E. 1992, MNRAS, 259, 345
Bender, R. 1990, A&A, 229, 441
Bottema, R. 1989, A&A, 221, 236
Bottema, R. 1993, A&A, 275, 16
Bottema, R., & Gerritsen, J. P. E. 1997, MNRAS, 290, 585
Buta, R., Combes, F. 1996, Fund. Cosmic Phys., 17, 95
Doyon, R., Joseph, R. D., & Wright, G. S. 1994, ApJ, 421, 101
De Jong, R. S. 1996, A&A, 313, 45
De Robertis, M. M., Yee, H. K., & Hayhoe, K. 1998, ApJ, 496, 93
Freeman, K. C. 1970, ApJ, 160, 811
Freeman, K. C. 1992, in Physics of Nearby Galaxies, Nature or Nurture? ed. T. X. Thuan, C. Balkowski, & T. T. Van (Ed. Frontières), 201
Friedli, D., & Benz, W. 1993, A&A, 268, 65
Friedli, D. 1996, A&A, 312, 761
Friedli, D., Wozniak, H., Rieke, M., Martinet, L., & Bratschi, P. 1996, A&AS, 118, 461

Gaffney, N. I., Lester, D. F., & Doppmann, G. 1995, PASP, 107, 68
Greusard, D., Friedli, D., Wozniak, H., Martinet, L., & Martin, P. 2000, A&A, 145, 425
Greusard, D., et al. 2001, in preparation, Paper II
Ho, L. C., Filippenko, A. V., & Sargent, W. L. 1997, ApJ, 487, 591
Jungwiert, B., Combes, F., & Axon, D. J. 1997, A&AS, 125, 479
Kalnajs, A. J. 1976, ApJ, 205, 745
Kotilainen, J. K., Forbes, D. A., Moorwood, A. F. M., et al. 1996, A&A, 313, 771
Kotilainen, J. K., Reunanen, J., Laine, S., & Ryder, S. D. 2000, A&A, 353, 834
Lindblad, P. O., & Lindblad, P. A. B. 1994, in Physics of the gaseous and stellar disks of the Galaxy, ed. I. King, PASP, 29
Lindblad, P. O. 1999, A&AR, 9, 221
Maiolino, R., Rieke, G. H., & Rieke, M. J. 1996, AJ, 111, 537
Mediavilla, E., & Arribas, S. 1995, MNRAS, 276, 579
Mulchaey, J. S., & Regan, M. W. 1997, ApJ, 482, L135
Pecontal, E., Adam, G., Bacon, R., et al. 1990, A&A, 232, 331
Prada, F., & Gutierrrez, C. M. 1999, ApJ, 517, 123 (PG99)
Regan, M. W., & Mulchaey, J. S. 1999, AJ, 117, 2676
Shaw, M. A., Combes, F., Axon, D. J., & Wright, G. S. 1993, A&A, 273, 31
Shlosman, I., Frank, J., & Begelman, M. C. 1989, Nature, 338, 45
Storchi-Bergmann, T., Wilson, A. S., & Baldwin, J. A. 1996, ApJ, 460, 252
Valentijn, E. A. 1990, Nature, 346, 153
Van der Kruit, P. C., & Searle, L. 1981, A&A, 95, 105 & 116
Van der Kruit, P. C., & Searle, L. 1982, A&A, 110, 61 & 79
Veron-Cetty, M., & Veron, P. 1993, ESO Scientific Report (Garching: ESO) –c1993, 6th ed.
Wada, K. 1994, PASJ, 46, 165
Wilson, A. S., Braatz, J. A., Heckman, T. M., Krolik, J. H., & Miley, G. K. 1993, ApJL, 419, L61
Wozniak, H., Friedli, D., Martinet, L., et al. 1995, A&AS, 111, 115